

Stable nanobubbles on ordered water monolayer near ionic model surfaces

Luyao Huang(黄璐瑶), Cheng Ling(凌澄), Limin Zhou(周利民), Wenlong Liang(梁文龙), Yujie Huang(黄雨婕), Lijuan Zhang(张立娟), Phornphimon Maitarad, Dengsong Zhang(张登松), and Chunlei Wang(王春雷)
Citation: Chin. Phys. B, 2025, 34 (**1**): 014701. DOI: 10.1088/1674-1056/ad989d

What follows is a list of articles you may be interested in

Morphological analysis for thermodynamics of cavitation collapse near fractal solid wall

Minglei Shan(单鸣雷), Yu Yang(杨雨), Xuefen Kan(阚雪芬), Cheng Yin(殷澄), and Qingbang Han(韩庆邦)
Chin. Phys. B, 2024, 33 (**6**): 064701. DOI: 10.1088/1674-1056/ad3343

Dynamic modeling of cavitation bubble clusters: Effects of evaporation, condensation, and bubble—bubble interaction

Long Xu(许龙), Xin-Rui Yao(姚昕锐), and Yang Shen(沈阳)
Chin. Phys. B, 2024, 33 (**4**): 044702. DOI: 10.1088/1674-1056/ad181f

Simulation of single bubble dynamic process in pool boiling process under microgravity based on phase field method

Chang-Sheng Zhu(朱昶胜), Bo-Rui Zhao(赵博睿), Yao Lei(雷瑶), and Xiu-Ting Guo(郭秀婷)
Chin. Phys. B, 2023, 32 (**4**): 044702. DOI: 10.1088/1674-1056/aca209

Nanobubbles produced by hydraulic air compression technique

Xiaodong Yang(杨晓东), Qingfeng Yang(杨庆峰), Limin Zhou(周利民),Lijuan Zhang(张立娟), and Jun Hu(胡钧)
Chin. Phys. B, 2022, 31 (**5**): 054702. DOI: 10.1088/1674-1056/ac464c

Investigation of cavitation bubble collapse in hydrophobic concave using the pseudopotential multi-relaxation-time lattice Boltzmann method

Minglei Shan(单鸣雷), Yu Yang(杨雨), Xuemeng Zhao(赵雪梦), Qingbang Han(韩庆邦), and Cheng Yao(姚澄)
Chin. Phys. B, 2021, 30 (**4**): 044701. DOI: 10.1088/1674-1056/abcf4b

---

RAPID COMMUNICATION

Stable nanobubbles on ordered water monolayer near ionic model surfaces

Luyao Huang(黄璐瑶)[1,2], Cheng Ling(凌澄)[3,4], Limin Zhou(周利民)[5], Wenlong Liang(梁文龙)[2], Yujie Huang(黄雨婕)[2], Lijuan Zhang(张立娟)[5], Phornphimon Maitarad[1,†], Dengsong Zhang(张登松)[2,‡], and Chunlei Wang(王春雷)[2,§]

[1] *Research Center of Nano Science and Technology, Department of Chemistry, College of Sciences, Shanghai University, Shanghai* 200444, *China*
[2] *International Joint Laboratory of Catalytic Chemistry, College of Sciences, Shanghai University, Shanghai* 200444, *China*
[3] *Shanghai Institute of Applied Physics, Chinese Academy of Sciences, Shanghai* 201800, *China*
[4] *University of Chinese Academy of Sciences, Beijing* 100049, *China*
[5] *Shanghai Synchrotron Radiation Facility, Shanghai Advanced Research Institute, Chinese Academy of Sciences, Shanghai* 201204, *China*

(Received 18 September 2024; revised manuscript received 28 October 2024; accepted manuscript online 29 November 2024)

The stable nanobubbles adhered to mineral surfaces may facilitate their efficient separation via flotation in the mining industry. However, the state of nanobubbles on mineral solid surfaces is still elusive. In this study, molecular dynamics (MD) simulations are employed to examine mineral-like model surfaces with varying degrees of hydrophobicity, modulated by surface charges, to elucidate the adsorption behavior of nanobubbles at the interface. Our findings not only contribute to the fundamental understanding of nanobubbles but also have potential applications in the mining industry. We observed that as the surface charge increases, the contact angle of the nanobubbles increases accordingly with shape transformation from a pancake-like gas film to a cap-like shape, and ultimately forming a stable nanobubble upon an ordered water monolayer. When the solid–water interactions are weak with a small partial charge, the hydrophobic gas (N_2) molecules accumulate near the solid surfaces. However, we have found, for the first time, that gas molecules assemble a nanobubble on the water monolayer adjacent to the solid surfaces with large partial charges. Such phenomena are attributed to the formation of a hydrophobic water monolayer with a hydrogen bond network structure near the surface.

Keywords: nanobubbles, molecular dynamic simulation, ordered water monolayer, hydrogen bond network

PACS: 47.55.dd, 87.10.Tf, 73.30.+y, 82.30.Rs

DOI: 10.1088/1674-1056/ad989d **CSTR:** 32038.14.CPB.ad989d

1. Introduction

Gas molecules confined to the nanoscale, with sizes smaller than 1 μm, exhibit properties distinct from those of macroscopic bubbles,[1–4] such as the unexpected long lifetime. An illustrative case is the generation of nanobubbles by electrochemical reactions,[5–7] where micro- and nanobubbles on the electrode surface can obstruct the active electrode area, resulting in increased overpotential and reduced current density.[8–13] Similarly, nanobubbles are widely used in the extraction of precious metals, rare earth elements, other minerals,[14–16] CO_2 hydrogenation and the materials fabrications.[17–19] Due to their small size, nanobubbles can effectively collide with and selectively adhere to mineral particles, an excellent application for separating target minerals.[20–25] Consequently, a deep understanding of the stability of nanobubbles may help improve electrode efficiency and enhance mineral flotation efficiency.[26–28]

Previous researchers have theoretically analyzed[29,30] and used molecular dynamic (MD) simulations[31,32] to predict that if the interior of nanobubbles has high density, their lifespan will be significantly extended. Subsequent researches have further demonstrated that the stability of nanobubbles is closely related to their high density,[33–35] interfacial interactions,[36–38] double-layer structure[39,40] and the surface hydrophobicity.[41,42] It has been generally acknowledged that the functional groups and charge distribution greatly determine surface hydrophilicity or hydrophobicity.[43–45] Some solid surfaces with hydrophilic groups, such as carboxyl, carbonyl, and hydroxyl groups,[46,47] can induce a hydration water film[48–54] that may hinder the direct adsorption of nanobubbles.[55–60] Thus, removing the hydration film may be necessary for nanobubbles to adsorb onto surfaces.[61,62] However, the exact form of nanobubbles adsorbed on these solid mineral surfaces remains unclear.

This paper aims to elucidate the adsorption behavior and stability of nanobubbles on various substrates with different hydrophobicity by using the MD simulations. There are four ionic surface models with surface charges of 0e, 0.5e, 0.7e and

†Corresponding author. E-mail: pmaitarad@shu.edu.cn
‡Corresponding author. E-mail: dszhang@shu.edu.cn
§Corresponding author. E-mail: wangchunlei1982@shu.edu.cn

© 2025 Chinese Physical Society and IOP Publishing Ltd. All rights, including for text and data mining, AI training, and similar technologies, are reserved.

1.0e. Surprisingly, our research demonstrated that nitrogen (N_2) nanobubbles can stably exist on the ordered water monolayer on the highly hydrophilic surfaces with a larger partial charge. By analyzing the formation of the water monolayer resulting from increased surface charge, along with changes in the contact angle and density of nanobubbles, we illustrated the formation mechanism of nanobubbles on different ionic surfaces. This study not only aids in understanding the microscopic stability of nanobubbles on different surfaces but also provides new theoretical insights for nanobubble assisted mineral flotation and materials science.

2. Simulation system and method

Full-atom MD simulations were performed to investigate the presence and morphology of nanobubbles on ionic surfaces by GROMACS 5.0.7.[63] The modeled theoretical surface, as illustrated in Fig. 1(a), has a base layer with dimensions of 6.395×6.816 nm^2 and a bond length of 0.142 nm between adjacent atoms. This model surface is believed to share similar water dynamic properties with ionic mineral surfaces. Positive and negative charges were evenly distributed along the diagonals of the hexagonal structure to ensure charge neutrality. This arrangement simulated the charge distribution characteristics observed on certain natural solid surfaces.[64] The Lennard–Jones (LJ) parameters were $\varepsilon = 0.121$ kJ/mol and $\sigma = 0.328$ nm.[65] The initial configuration is shown in Fig. 1(b), with a z-axis length of 6.5 nm. Herein, 400 nitrogen molecules were randomly distributed within the simulation box. The box was filled with 8093 water molecules using the SPC/E model, maintaining a saturation ratio of water to nitrogen at 20:1. The LJ parameters for nitrogen atoms were $\varepsilon = 0.711$ kJ/mol and $\sigma = 0.325$ nm.[65,66] All the LJ parameters used in our simulations are extensively employed in MD simulations. These parameters have been validated and can reproduce and observe material characteristics such as the phase diagram of liquid nitrogen, the Henry's law constant for nitrogen in water, the contact angle between water droplets and graphite, and the isotherm of nitrogen on graphite.[65–67] Additionally, we conducted simulations of the ionic solid surface in a gas-free liquid environment containing 8693 water molecules. This setup enables a comparative analysis of the impact of nanobubbles on the surface.

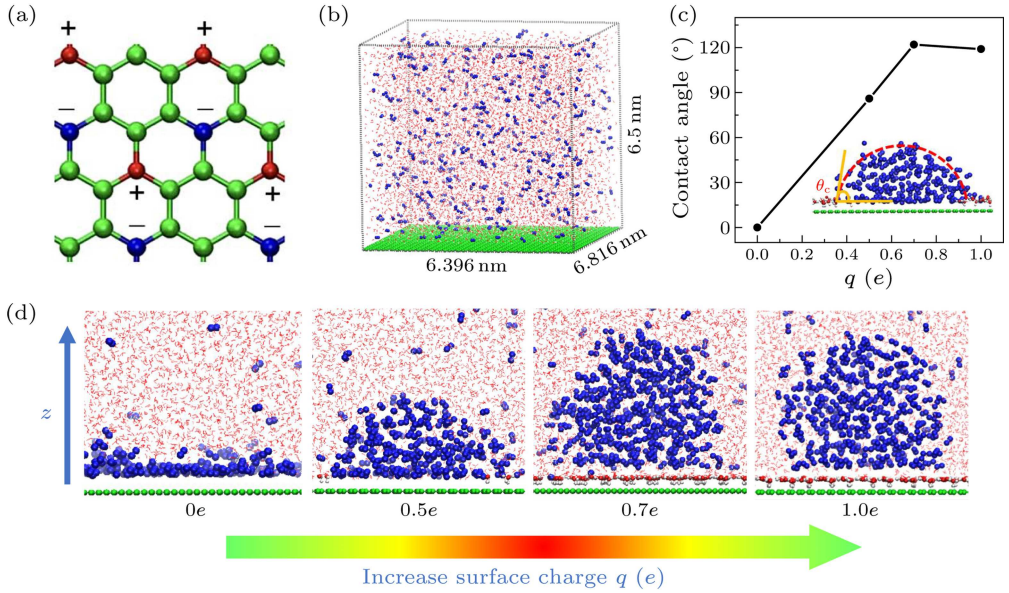


Fig. 1. (a) Geometry of the ionic solid model. Red and blue spheres represent atoms with positive and negative charges, respectively, while green spheres represent neutral atoms. (b) Initial structure of the simulation box. The green and blue spheres represent solid atoms and nitrogen gas molecules, respectively. While the red dots represent water molecules. (c) The contact angle θ_c of surface nanobubbles as a function of q, along with an illustration of θ_c. (d) Gas aggregation patterns on differently charged model surfaces. The 0.7e and 1.0e solid surfaces have a water layer, with red spheres representing O and white spheres representing H.

Periodic boundary conditions were applied in all directions. The simulation was performed in the NVT ensemble, with temperature maintained at 300 K using a Nose–Hoover thermostat and a coupling time of 0.2 ps. Van der Waals interactions and short-range electrostatic interactions were calculated using a cutoff distance of 1 nm. Long-range electrostatic interactions were managed using the particle mesh Ewald method with a real-space cutoff of 1 nm. The timestep was set to 1 fs, and the total simulation time was 20 ns. Structural analysis was performed on the data from the last 2 ns of the simulation. Each simulation was repeated three times.

To estimate the contact angle of the nanobubbles, we established the boundary of the gas–liquid interface based on a density distribution method. In practice, the simulation box was divided into equal-volume cells, each with a side length of 0.3 nm. The number density of nitrogen molecules in these

cells was calculated every 10 frames. The position where the average gas density was about half of the maximum density was identified as the gas–liquid interface. Subsequently, the contact angle was determined by fitting the data to a circle using the following geometric calculations:[68]

$$\theta_c = \arccos\frac{R - Z_{max}}{R}, \quad (Z_{max} < R), \tag{1}$$

$$\theta_c = 90^\circ + \arccos\frac{Z_{max} - R}{R}, \quad (Z_{max} > R). \tag{2}$$

Here, θ_c denotes the contact angle, R represents the radius of the fitted circle, and Z_{max} is the highest coordinate of the fitted circle. By averaging the last 2 ns, we obtained the contact angle of the nanobubble.

3. Results and discussion

3.1. The aggregation state of nanobubbles on different model surfaces

To investigate the aggregation patterns of nanobubbles on charged ionic surfaces, four surface models were constructed with different values of positive and negative charges, as illustrated in Fig. 1(a), with charges of 0e, 0.5e, 0.7e, and 1.0e, respectively. The stabilized configuration was extracted after 20 ns of simulation. Figure 1(c) shows the change in the contact angle θ_c of nanobubbles with varying q, and Fig. 1(d) illustrates the structure and adsorption of gases on the surfaces of the models with different charges. Initially, gas molecules form a pancake-like gas film on the $q = 0e$ surface with a θ_c of 0°. As the charge increases to 0.5e, they gradually accumulate into cap-shaped nanobubbles with a θ_c of $86^\circ \pm 2^\circ$. At $q = 0.7e$, the gas molecules form spherical clusters on the surface, having a θ_c of $122^\circ \pm 2^\circ$. At $q = 1.0e$, the clusters become more perfectly spherical, with a θ_c of $119^\circ \pm 8^\circ$. Our analysis revealed that as the charge increases, nanobubbles gradually form, and the contact angle increases accordingly. Notably, when $q \geq 0.7e$, a water layer exists between the solid surface and the nanobubbles. This behavior suggests that nanobubbles are not in direct contact with the surface. Instead, they adhere to the interfacial water layer and are stabilized against the surface. Recently, Niwano *et al.*[69] detected absorption peaks of interfacial water between nanobubbles and solid substrates, suggesting that the structure of this interfacial water may consist of ternary, quaternary, or pentameric water clusters. Similar evidence is shown in the interfacial monolayer water structure in Fig. 3(c).

We counted the numbers of water and nitrogen molecules within 0.4 nm of the interface as a function of q, as shown in Fig. 2(a). With increasing q, the number of nitrogen molecules decreases while the number of water molecules increases, consistent with the simulation results in Fig. 1(d). When $q \geq 0.7e$, gas molecules are replaced by water molecules. The electrostatic interactions between the surface charge and polar water molecules drive this phenomenon. As the charge increases, these solid–water interactions become stronger, which results in more water molecules enriching onto the solid surface and repelling gas molecules.

The density of nanobubbles was estimated to investigate the impact of different surface partial charges on their formation and state. As shown in Fig. 2(b), under different charge conditions, the nanobubble density shows a distinct peak, indicating the formation of a dense gas-enrichment layer, similar to the gas adsorption structure observed in previous works.[70–72] The results demonstrate that as q increases from 0e to 0.7e, the density of the first peak in the nitrogen density profile, corresponding to the gas adsorption layer, gradually decreases from 748.60 kg/m^3 to 124.77 kg/m^3. As the charge continually increases to 1.0e, the density changes slightly. Notably, when the water monolayer appears ($q \geq 0.7e$), the density of the gas-enrichment layer significantly decreases. This high-density gas layer on the surface may be a key factor in maintaining the stability of nanobubbles, as it not only effectively alters the chemical properties of the substrate but also compensates for the release of gas within the nanobubbles.[51,52] When the density of this layer reaches a certain level, nanobubbles can maintain dynamic stability.[73,74] These simulation results indicate that the adsorption state of gases on the surface is closely related to the ionic surface charge.

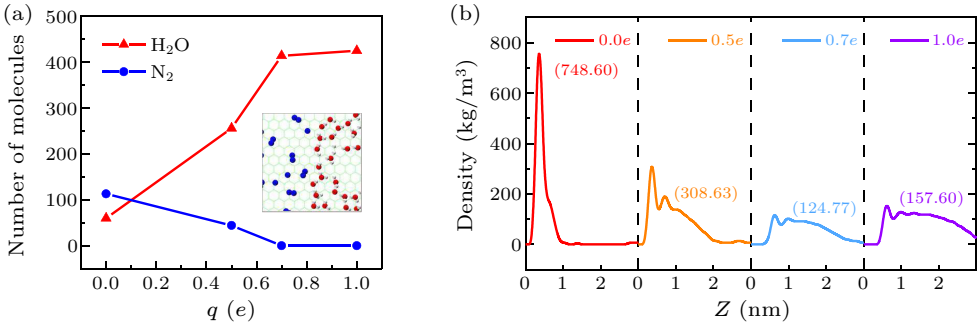


Fig. 2. (a) The numbers of nitrogen and water molecules within 0.4 nm of the solid surface as a function of q, along with an illustration of water and nitrogen molecules within 0.4 nm of the surface. Green lines represent C–C bonds, while blue, red, and white spheres represent N, O, and H, respectively. (b) The gas density of nanobubbles from the interface as a function of q.

3.2. Stable nanobubbles on ordered water monolayer

To explore why nanobubbles remain stable in the presence of a water layer, we selected the simulation results at $q = 1.0e$ for further analysis. We calculated the ratio of the number of molecules inside and outside the nanobubbles to the total number of nitrogen molecules over the simulation time. We consider a gas molecule inside a nanobubble if there are more than 10 gas molecules within a radius of 1 nm from its center. Otherwise, it is considered to be in the water phase. As shown in Fig. 3(a), gas molecules rapidly form a nanobubble, reaching equilibrium around 5 ns, with the nanobubble stabilizing on the surface of the water layer. Subsequently, to estimate the density distribution of water molecules along the z-axis, the x–z plane was divided into 130 rectangular bins. The relative mass density of water molecules in each bin was calculated, with the bulk water density of 0.997 g/cm^3. The results, as shown in Fig. 3(b), demonstrate that the water molecules at the first peak form a high-density layer. Based on the density profile's peaks and troughs, the water layer is 0.4 nm thick, approximately the thickness of a monolayer of molecules. We also found that the water monolayer under the nanobubble exhibits a more ordered hydrogen bond (H-bond) network structure compared to the monolayer outside the nanobubble, forming a distinctive hexagonal H-bond network [Fig. 3(c)]. The special arrangement of charges on the ionic surface influences the formation of the two-dimensional water structure and the distribution of the H-bond network, accounting for this phenomenon.[64] Additionally, the nanobubble hinders H-bond formation between the water monolayer and bulk water, resulting in a more ordered H-bond network under the nanobubble.

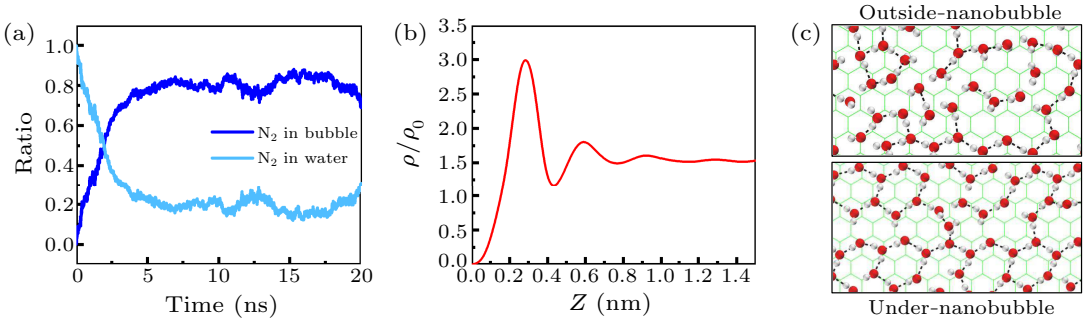


Fig. 3. Simulation results when the partial charge $q = 1.0e$. (a) The ratio of gas molecules inside nanobubbles over simulation time. (b) Density distribution of water molecules on the solid surface along the z-axis. (c) A snapshot of the water monolayer molecules. The top panel illustrates the water monolayer outside the nanobubble, while the bottom panel shows the water monolayer under the nanobubble, with hydrogen bonds (black dashed lines) between adjacent molecules.

Why do surface nanobubbles persist on this ordered water monolayer surface with a larger surface partial charge? We attribute the formation to this water layer's distinctive hydrogen bond (H-bond) structure. To further elucidate the structure of interfacial water beneath the nanobubbles, we estimated the average number of H-bonds formed within the water monolayer molecules when the surface $q \geq 0.7e$. The criteria for H-bond formation between two water molecules are established using a set of standard parameters. If the O–O distance between two water molecules is less than 0.35 nm, and the $\angle$HO$\cdots$O is less than 30°, a H-bond is considered to be formed. As shown in Table 1, in the absence of nanobubbles, the average number of hydrogen bonds within the water monolayer molecules gradually increases as the surface charge increases. Consistent with previous research,[64,75] we have found that the number of H-bonds within the water monolayer increases from 2.18 for $q = 0.7e$ to 2.28 for $q = 1.0e$. Then, the number of H-bonds between the monolayer and bulk water decreases, leading to a certain degree of hydrophobicity in the monolayer. Evidently, hydrophobic gas molecules (N_2) form a gas-enrichment layer on the water monolayer due to the hydrophobicity of the water monolayer. As more gas molecules accumulate on this layer, nanobubbles eventually form. We also analyzed the changes in the number of hydrogen bonds within the water monolayer molecules in the presence of nanobubbles. The results show that under the same charge, the average number of hydrogen bonds within the water monolayer also increases, i.e., from 2.18 to 2.23 for $q = 0.7e$ and from 2.28 to 2.35 for $q = 1.0e$, respectively. This shows that the presence of nanobubbles stabilizes the two-dimensional hydrogen bonds within the water monolayer. The results indicate that the surface nanobubbles can increase the hydrophobicity of particles.

Table 1. The average number of hydrogen bonds within the water monolayer molecules changes with surface charge q.

Charge (e)	Without nanobubble	With nanobubble
0.7	2.18	2.23
1.0	2.28	2.35

4. Conclusions

In summary, we employed molecular dynamics (MD) simulations to investigate the adsorption states of gas

molecules on ionic surfaces with varying partial charges. As surface charges gradually increased from 0e to 1.0e, the contact angle of the nanobubbles increased from 0° to 119° ± 8°, eventually forming spherical nanobubbles. Our observations revealed that on some ionic surfaces with more significant partial charges, nanobubbles stably exist upon an ordered water monolayer adsorbed on the solid substrate. Through computational analysis, as the surface charge increases, the average number of hydrogen bonds within the water monolayer molecules increases, leading to a more stable hydrogen bond network within the water monolayer. This induces the hydrophobicity of the water monolayer and promotes the stable existence of nanobubbles with hydrophobic gas molecules accumulation near the water monolayer.

This finding enhances our understanding of nanobubble adsorption on solid surfaces with varying degrees of hydrophobicity and hydrophilicity. Considering the general existence of the hydrophobic water monolayer on the mineral/oxide/metal surfaces, we expect that this new three-phase state on the solid surfaces will inspire more experiments in this direction. It may provide a theoretical foundation for improving the efficiency of mineral flotation, materials fabrication, and nanobubble generation in water electrolysis.

Acknowledgements

This study was supported by the National Natural Science Foundation of China (Grant Nos. 12022508, 12074394, and 22125604), Shanghai Supercomputer Center of China, and Shanghai Snowlake Technology Co. Ltd.

References

[1] Ishida N, Inoue T, Miyahara M and Higashitani K 2000 *Langmuir* **16** 6377
[2] Temesgen T, Bui T T, Han M, Kim T I and Park H 2017 *Adv. Colloid Interface Sci.* **246** 40
[3] Yang X, Yang Q, Zhou L, Zhang L and Hu J 2022 *Chin. Phys. B* **31** 054702
[4] Wen B, Pan Y, Zhang L, Wang S, Zhou L, Wang C and Hu J 2022 *Phys. Rev. Fluids* **7** 103601
[5] Zhang L, Zhang Y, Zhang X, Li Z, Shen G, Ye M, Fan C, Fang H and Hu J 2006 *Langmuir* **22** 8109
[6] Chen Q, Wiedenroth H S, German S R and White H S 2015 *J. Am. Chem. Soc.* **137** 12064
[7] Lu D 2024 *The Innovation* **5** 100646
[8] Vogt H and Balzer R J 2005 *Electrochim. Acta* **50** 2073
[9] Angulo A, van der Linde P, Gardeniers H, Modestino M and Fernández Rivas D 2020 *Joule* **4** 555
[10] Zhao X, Ren H and Luo L 2019 *Langmuir* **35** 5392
[11] Seh Z W, Kibsgaard J, Dickens C F, Chorkendorff I, Nørskov J K and Jaramillo T F 2017 *Science* **355** eaad4998
[12] Ma Y, Guo Z, Chen Q and Zhang X 2021 *Langmuir* **37** 2771
[13] Chen Q, Zhao J, Deng X, Shan Y and Peng Y 2022 *J. Phys. Chem. Lett.* **13** 6153
[14] Marion C, Li R and Waters K E 2020 *Adv. Colloid Interface Sci.* **279** 102142
[15] Ren L, Zhang Z, Zeng W and Zhang Y 2023 *Int. J. Min. Sci. Technol.* **33** 503
[16] Zhao Y, Jia J, Liu C and Feng X 2024 *The Innovation* **5** 100576
[17] Li H, Fang W, Wang L X, Liu Y, Liu L, Sun T, Liao C, Zhu Y, Wang L and Xiao F S 2023 *The Innovation* **4** 100445
[18] Xiang M, Shen Z, Zheng J, Song M, He Q, Yang Y, Zhu J, Geng Y, Yue F, Dong Q, Ge Y, Wang R, Wei J, Wang W, Huang H, Zhang H, Zhu Q and Zhang C J 2024 *The Innovation* **5** 100540
[19] Zhang W, Shao Y, Zou X, Yan J, Xu M, Zhou G and Fu S 2024 *The Innovation* **5** 100642
[20] Sobhy A and Tao D 2013 *Int. J. Miner. Process.* **124** 109
[21] Wang Y, Pan Z, Luo X, Qin W and Jiao F 2019 *Miner. Eng.* **133** 127
[22] Zhou W, Chen H, Ou L and Shi Q 2016 *Int. J. Miner. Process.* **157** 236
[23] Zhang N, Pang T, Han R, Chen S, Li Z, Yu Y, Shi Z, Liu L, Qu J and Zhou A 2022 *Int. J. Min. Sci. Technol.* **32** 201
[24] Alheshibri M, Al Baroot A, Shui L and Zhang M 2021 *Curr. Opin. Colloid Interface Sci.* **55** 101470
[25] Zhang L, Zhang X, Zhang Y, Hu J and Fang H 2010 *Soft Matter* **6** 4515
[26] Maheshwari S, van der Hoef M, Zhang X and Lohse D 2016 *Langmuir* **32** 11116
[27] Perez Sirkin Y A, Gadea E D, Scherlis D A and Molinero V 2019 *J. Am. Chem. Soc.* **141** 10801
[28] Zhang F, Cai H, Fan G, Gui X, Xing Y and Cao Y 2024 *Colloids Surf. A* **699** 134633
[29] Zhang L, Chen H, Li Z, Fang H and Hu J 2008 *Sci. China Phys. Mech.* **51** 219
[30] Weijs J H and Lohse D 2013 *Phys. Rev. Lett.* **110** 054501
[31] Wang C L, Li Z X, Li J Y, Xiu P, Hu J and Fang H P 2008 *Chin. Phys. B* **17** 2646
[32] Wang Z, Yang L, Liu C and Lin S 2023 *Chin. Phys. B* **32** 023101
[33] Zhou L, Wang X, Shin H J, Wang J, Tai R, Zhang X, Fang H, Xiao W, Wang L, Wang C, Gao X, Hu J and Zhang L 2020 *J. Am. Chem. Soc.* **142** 5583
[34] Gao Z, Wu W, Sun W and Wang B 2021 *Langmuir* **37** 11281
[35] Hu K, Luo L, Sun X and Li H 2022 *Nanoscale Adv.* **4** 2893
[36] Yen T H, Lin C H and Chen Y L 2021 *Langmuir* **37** 2759
[37] Maheshwari S, van der Hoef M, Rodríguez Rodríguez J and Lohse D 2018 *ACS Nano* **12** 2603
[38] Lan L, Pan Y, Zhou L, Kuang H, Zhang L and Wen B 2025 *J. Colloid Interface Sci.* **678** 322
[39] Lei J, Huang D, Zhao W, Liu S and Yue Y 2024 *Int. J. Heat Mass Transfer* **225** 125407
[40] Zhang P, Chen C, Feng M, Sun C and Xu X 2024 *J. Am. Chem. Soc.* **146** 19537
[41] Desgranges C and Delhommelle J 2019 *J. Phys. Chem. C* **123** 11707
[42] Attard P 2003 *Adv. Colloid Interface Sci.* **104** 75
[43] Qu M, Huang G, Liu X, Nie X, Qi C, Wang H, Hu J, Fang H, Gao Y, Liu W T, Francisco J S and Wang C 2022 *Chem. Sci.* **13** 10546
[44] Zhao Z, Park J, Choi C, Hong S, Hui X, Zhang H, Benedict Lo T W, Robertson A W, Lv Z, Jung Y and Sun Z 2022 *The Innovation* **3** 100190
[45] Hou L, Liu X, Ge X, Hu R, Cui Z, Wang N and Zhao Y 2023 *The Innovation* **4** 100508
[46] Wang S, Tang L and Tao X 2018 *Fuel* **212** 326
[47] Chang Z, Chen X and Peng Y 2017 *Powder Technol.* **321** 190
[48] Abel M, Clair S, Ourdjini O, Mossoyan M and Porte L 2011 *J. Am. Chem. Soc.* **133** 1203
[49] Yuan Q and Zhao Y P 2010 *Phys. Rev. Lett.* **104** 246101
[50] Phan A, Ho T A, Cole D R and Striolo A 2012 *J. Phys. Chem. C* **116** 15962
[51] Lützenkirchen J, Zimmermann R, Preočanin T, Filby A, Kupcik T, Küttner D, Abdelmonem A, Schild D, Rabung T, Plaschke M, Brandenstein F, Werner C and Geckeis H 2010 *Adv. Colloid Interface Sci.* **157** 61
[52] Lee K, Kim Q, An S, An J, Kim J, Kim B and Jhe W 2014 *Proc. Natl. Acad. Sci. USA* **111** 5784
[53] Zhang J, Tan J, Pei R, Ye S and Luo Y 2021 *J. Am. Chem. Soc.* **143** 13074
[54] Wang Y H, Zheng S, Yang W M, Zhou R Y, He Q F, Radjenovic P, Dong J C, Li S, Zheng J, Yang Z L, Attard G, Pan F, Tian Z Q and Li J F 2021 *Nature* **600** 81
[55] Shen L, Wang C, Min F, Liu L and Xue C 2020 *Fuel* **271** 117557
[56] Xia W 2017 *Int. J. Miner. Process.* **168** 19
[57] Chen Y, Xia W and Xie G 2018 *Fuel* **222** 35
[58] Gao L X, Li X G, Lyu X J and Zhu X N 2024 *Energy Fuels* **38** 1566
[59] Xia Y, Zhang R, Cao Y, Xing Y and Gui X 2020 *Fuel* **262** 116535
[60] Li M, Xing Y, Zhu C, Liu Q, Yang Z, Zhang R, Zhang Y, Xia Y and Gui X 2022 *Int. J. Min. Sci. Technol.* **32** 1389

[61] Li B, Su D, Che D, Zhang L, Liu S and Albijanic B 2024 *Miner. Eng.* **209** 108610
[62] Xia Y, Zhang R, Xing Y and Gui X 2019 *Fuel* **235** 687
[63] Abraham M J, Murtola T, Schulz R, Páll S, Smith J C, Hess B and Lindahl E 2015 *SoftwareX* **1** 19
[64] Wang C, Lu H, Wang Z, Xiu P, Zhou B, Zuo G, Wan R, Hu J and Fang H 2009 *Phys. Rev. Lett.* **103** 137801
[65] Wang S, Zhou L, Wang X, Wang C, Dong Y, Zhang Y, Gao Y, Zhang L and Hu J 2019 *Langmuir* **35** 2498
[66] Wang S, Hou K and Heinz H 2021 *J. Chem. Theory Comput.* **17** 5198
[67] Vernov A V and Steele W A 1986 *Langmuir* **2** 219
[68] Scocchi G, Sergi D, D'Angelo C and Ortona A 2011 *Phys. Rev. E* **84** 061602
[69] Niwano M, Ma T, Iwata K, Tadaki D, Yamamoto H, Kimura Y and Hirano-Iwata A 2023 *J. Colloid Interface Sci.* **652** 1775
[70] Li C, Wang S P, Zhang A M and Liu Y 2018 *Phys. Rev. Fluids* **3** 123604
[71] Yang H, Jiang H, Cheng Y, Xing Y, Cao Y and Gui X 2024 *J. Mol. Liq.* **411** 125758
[72] Varghese B and Sathian S P 2022 *Phys. Chem. Chem. Phys* **24** 22298
[73] Weijs J H, Snoeijer J H and Lohse D 2012 *Phys. Rev. Lett.* **108** 104501
[74] Brenner M P and Lohse D 2008 *Phys. Rev. Lett.* **101** 214505
[75] Qi C, Ling C and Wang C 2023 *Crystals* **13** 263